Geometrical effects on the thermoelectric properties of ballistic graphene antidot lattices

Hossein Karamitaheri,[1] Mahdi Pourfath,[2,3,a)] Rahim Faez,[1] and Hans Kosina[3]
[1]*School of Electrical Engineering, Sharif University of Technology, Tehran 11365-9363, Iran*
[2]*Electrical and Computer Engineering Department, University of Tehran, Tehran 14395-515, Iran*
[3]*Institute for Microelectronics, Technische Universität Wien, Gußhausstraße 27-29/E360, A-1040 Wien, Austria*

(Received 12 April 2011; accepted 19 July 2011; published online 7 September 2011)

The thermoelectric properties of graphene-based antidot lattices are theoretically investigated. A third nearest-neighbor tight-binding model and a fourth nearest-neighbor force constant model are employed to study the electronic and phononic band structures of graphene antidot lattices with circular, rectangular, hexagonal, and triangular antidot shapes. Ballistic transport models are used to evaluate transport coefficients. Methods to reduce the thermal conductance and to increase the thermoelectric power factor of such structures are studied. Our results indicate that triangular antidot lattices have the smallest thermal conductance due to longer boundaries and the smallest distance between the neighboring antidots. Among them, iso-triangular antidot lattices have also a large power factor and as a result a large figure of merit. © *2011 American Institute of Physics*. [doi:10.1063/1.3629990]

I. INTRODUCTION

Today, thermoelectric devices can be used in a very wide range of applications including energy harvesting, aerospace, and military applications. The thermoelectric figure of merit is defined as

$$ZT = \frac{S^2 GT}{(K_{el} + K_{ph})}, \quad (1)$$

where S, G, T, K_{el}, and K_{ph} are the Seebeck coefficient, the electrical conductance, temperature, and the electrical and lattice contributions to the thermal conductance, respectively.[1] The numerator of Z is called power factor. The figure of merit determines the efficiency of a thermoelectric device and can be improved by increasing the power factor and decreasing the thermal conductance. Hence, thermoelectric materials must simultaneously have a high Seebeck coefficient, a high electrical conductance, and a low thermal conductance.

While each property of ZT can individually be changed by several orders of magnitude, the interdependence and coupling between these properties have made it extremely difficult to increase $ZT > 1$. Bismuth and its alloys that are commonly used in thermoelectric applications[2] suffer from high cost. On the contrary, bulk silicon has a very low $ZT \approx 0.01$ (Ref. 3) because of its high thermal conductance.

In recent years many studies have been conducted for employing new materials and technologies to improve ZT. Progress in nanomaterials synthesis has allowed the realization of low-dimensional thermoelectric device structures such as one-dimensional nanowires, thin films, and two-dimensional superlattices.[4–6] However, the recent breakthroughs in materials with $ZT > 1$ have mainly benefited from reduced phonon thermal conductance.[6,7]

Graphene, a recently discovered form of carbon, has received much attention over the past few years due to its excellent electrical, optical, and thermal properties.[8] The electrical conductance of graphene is as high as that of copper.[9] As a zero band-gap material, pristine graphene has a small Seebeck coefficient.[10] However, one can open up band-gaps by appropriate patterning of graphene sheets.[11–13] Graphene nanoribbons (GNRs) are thin strips of graphene, where the band-gap is varied by the chirality of the edge and the width of ribbon. Zigzag GNRs show metallic behavior, whereas armchair GNRs are semiconductors and their band-gap is inversely proportional to the width.[11] Very recently, Zhang and co-workers showed that one can open up a significant band-gap in zigzag GNRs by edge manipulation.[14] In addition, it has been theoretically[15] and experimentally[16] shown that by introducing regular holes into the graphene sheet, an energy band-gap can be achieved. On the other hand, a large scale method to produce graphene sheets has been reported.[17] These factors render graphene as a candidate for future thermoelectric applications.

However, the ability of graphene to conduct heat is an order of magnitude higher than that of copper.[18] Therefore, it is necessary to reduce its thermal conductance. The high thermal conductance of graphene is mostly due to the lattice contribution, whereas the electronic contribution to the thermal conduction can be ignored.[18,19] Therefore, by proper engineering of phonon transport it is possible to reduce the total thermal conductance without significant reduction of the electrical conductance and the power factor.

Recently many theoretical studies have been performed on the thermal conductivity of graphene-based structures. It has been shown that boundaries and edge roughness can strongly influence the thermal conductance.[20] Uniaxial strain can remarkably decrease the thermal conductance of GNRs.

[a)]Electronic mail: pourfath@iue.tuwien.ac.at.

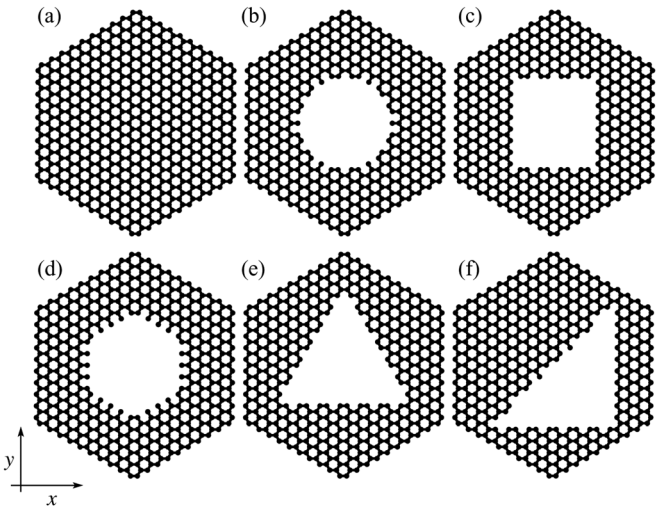

FIG. 1. Geometrical structures of different GALs. (a)-(f) indicate pristine graphene, Circ(10, 108), Rect(10, 120), Hex(10, 120), IsoTri(10, 126), and RightTri(10, 126), respectively. Transport is assumed to be in the direction of the x-axis.

In the case of zigzag GNRs, 15% uniaxial strain can decrease the thermal conductance to one fifth of that of an unstrained GNR.[21] Vacancy, defects, and isotope doping have magnificent effects on thermal conductance.[22,23] Furthermore, it has been recently shown that the thermal conductance of GNRs can be reduced by hydrogen-passivation of the edges.[24] In this work we investigate the ballistic thermoelectric properties of a new graphene-based structure, which is called graphene antidot lattice (GALs).[16] Although the electrical and thermal carriers scattering play an important role in thermoelectric properties of materials, the ballistic results give us an insight into how these new materials can be used in the future thermoelectric applications. We show that by introducing antidots in the graphene sheet (Fig. 1) the thermal conductances of GALs decrease and the respective ZT values increase.

II. GRAPHENE ANTIDOT LATTICES

The electrical and optical properties of GALs have been theoretically studied in Refs. 12, 15, and 25. The results indicate that by introducing regular antidots in a graphene sheet, it is possible to achieve a direct band-gap semiconductor from a semi-metal pristine graphene sheet. Bai and co-workers reported the first field-effect-transistor based on GALs.[16] In this paper we investigate the effect of the dot geometry on the thermoelectric properties of GALs. The unit cell of a GAL can be described by two parameters L and N, where L is the side length of the hexagon in terms of the graphene lattice constant ($a = 2.46\mathring{A}$) and N is the number of carbon atoms that are removed from the pristine supercell. In Fig. 1 Circ, Rect, Hex, IsoTri, and RightTri represent a circular, rectangular, hexagonal, iso-triangular, and right-triangular antidot in the hexagonal unit cell, respectively. Figure 1(b) shows a circular antidot that is formed by removing 108 carbon atoms from a cell with $L = 10$. It is therefore represented by Circ(10, 108). The number of edge carbon atoms in a unit cell of different GALs is also given in Table I. As we will show later the number of carbon atoms at the boundary plays an important role on the thermal properties of the structure.

TABLE I. The number of edge carbon atoms in a unit cell of different GALs.

Structure	Number of boundary atoms
Circ(10, 108)	30
Rect(10, 120)	32
Hex(10, 120)	30
IsoTri(10, 126)	36
RightTri(10, 126)	38

III. APPROACH

The electronic and phononic band structures are evaluated using a third nearest-neighbor tight-binding and a fourth nearest-neighbor force constant method, respectively. Using the band structures, the ballistic transmission that is equal to the density of modes $M(E)$ is evaluated.[26] Finally, the transport coefficients are calculated by employing a ballistic transport model.

A. Band structure calculations

To describe the electronic band structure of GALs, a third nearest-neighbor tight-binding approximation is employed.[27] The hopping parameters for the first, second, and third nearest-neighbor are assumed to be -3.2 eV, 0 eV, and -0.3 eV, respectively.[27]

A dynamical matrix can be used to describe the dispersion relation of phonons:

$$D^{ij}(k) = \left(\sum_l K^{il} - M_i\omega^2(k)I\right)\delta_{ij} - \sum_l K^{il}e^{ik\cdot\Delta R_{il}} \quad (2)$$

where M_i is the atomic mass of the ith carbon atom, $\mathbf{\Delta R}_{ij} = \mathbf{R}_i - \mathbf{R}_j$ is the distance between the ith and the jth carbon atoms, and K^{ij} is a 3×3 force constant tensor describing the coupling between the ith and the jth carbon atoms, which are the Nth nearest-neighbor of each other:

$$K^{(ij)} = U_m^{-1}\begin{pmatrix} \Phi_r^{(N)} & 0 & 0 \\ 0 & \Phi_{ti}^{(N)} & 0 \\ 0 & 0 & \Phi_{to}^{(N)} \end{pmatrix} U_m. \quad (3)$$

Φ_r, Φ_{ti}, and Φ_{to} are the radial, the in-plane transverse, and the out-of-plane transverse components of the force constant tensor, respectively. Their values are given in Table II.[28] U_m is a unitary matrix defined as

$$U_m = \begin{pmatrix} \cos\Theta_{ij} & \sin\Theta_{ij} & 0 \\ -\sin\Theta_{ij} & \cos\Theta_{ij} & 0 \\ 0 & 0 & 1 \end{pmatrix}. \quad (4)$$

Here, we assume that the graphene sheet is located in the x-y plane and Θ_{ij} represents the angle between the x-axes and the bond between the ith and jth carbon atoms.

TABLE II. The elements of the force constant tensor in *N*/m (Ref. 35).

N	Φ_r	Φ_{ti}	Φ_{to}
1	365.0	245.0	98.2
2	88.0	−32.3	−4.0
3	30.0	−52.5	1.5
4	−19.2	22.9	−5.8

B. Transport coefficients

According to the Landauer formalism,[29] the electric current and heat current can be calculated as a function of the electron and phonon transmissions. In the linear response regime, the electrical and heat currents are proportional to the applied voltage, when the temperature difference is zero. They are also proportional to the temperature difference, if the voltage is zero. Therefore, in the linear response regime, these currents are expressed as

$$I = G\Delta V + \overline{SG}\Delta T, \tag{5}$$

$$I_q = -T\overline{SG}\Delta V - K_0\Delta T, \tag{6}$$

where I and I_q are the electric and heat currents, respectively. Here, G is the electrical conductance and K_0 is the electronic contribution to the thermal conductance for zero electric field:[30]

$$G = \frac{2q^2}{h}\int_{-\infty}^{+\infty}\overline{T}_{\mathrm{el}}(E)\left(-\frac{\partial f}{\partial E}\right)dE, \tag{7}$$

$$K_0 = \frac{2}{hT}\int_{-\infty}^{+\infty}\overline{T}_{\mathrm{el}}(E)(E-E_{\mathrm{F}})^2\left(-\frac{\partial f}{\partial E}\right)dE, \tag{8}$$

where $\overline{T}_{\mathrm{el}}(E)$ is the electron transmission and h is the Planck's constant. As we show later, the proportionality factor of ΔT in Eq. (5) is equal to the product SG, so we represent this factor by $\overline{SG}$. Similarly, the proportionality factor of ΔV in Eq. (6) is represented by $-T\overline{SG}$. One can simply rewrite Eqs. (7) and (8) as[30,31]

$$\Delta V = I/G - S\Delta T, \tag{9}$$

$$I_q = \Pi I - K_{\mathrm{el}}\Delta T, \tag{10}$$

where $\Pi = -TS$ is the Peltier coefficient and $K_{\mathrm{el}} = K_0 - TS^2G$. One can evaluate the Seebeck coefficient $S = \overline{SG}/G$ as[30]

$$S = \left(\frac{k_{\mathrm{B}}}{-q}\right)\frac{\int_{-\infty}^{+\infty}\overline{T}_{\mathrm{el}}(E)[(E-E_{\mathrm{F}})/k_{\mathrm{B}}T]\left(-\frac{\partial f}{\partial E}\right)dE}{\int_{-\infty}^{+\infty}\overline{T}_{\mathrm{el}}(E)\left(-\frac{\partial f}{\partial E}\right)dE}, \tag{11}$$

where k_{B} is the Boltzmann constant and E_{F} is the Fermi-level of the system. In Eqs. (7), (8), and (11), the derivative of the Fermi function

$$-\frac{\partial f}{\partial E} = \frac{1}{4k_{\mathrm{B}}T}\left[\cosh\left(\frac{E-E_{\mathrm{F}}}{k_{\mathrm{B}}T}\right)\right]^{-2} \tag{12}$$

is known as the thermal broadening function. It has a width of a few $k_{\mathrm{B}}T$ around E_{F}.

Within the framework of the Landauer theory, one can express the lattice contribution to the thermal conductance as[22]

$$K_{\mathrm{ph}} = \frac{1}{h}\int_0^{+\infty}\overline{T}_{\mathrm{ph}}(\omega)\hbar\omega\left(\frac{\partial n(\omega)}{\partial T}\right)d(\hbar\omega), \tag{13}$$

where $n(\omega)$ denotes the Bose-Einstein distribution function and $\overline{T}_{\mathrm{ph}}(\omega)$ is the phonon transmission. In the ballistic limit, $\overline{T}_{\mathrm{el,ph}}(E)$ can be extracted from the density of modes $M(E)$[30]

$$\overline{T}_{\mathrm{el,ph}}(E)|_{\mathrm{Ballistic}} = M_{\mathrm{el,ph}}(E) = \sum_{k_\perp}\Theta[E-\varepsilon_{\mathrm{el,ph}}(k_\perp)], \tag{14}$$

where Θ is the unit step function and $k_\perp$ refers to the wave vector component perpendicular to the transport direction.[30]

IV. RESULTS AND DISCUSSION

The Seebeck coefficient and power factor are sensitive to the details of the density of states and the asymmetry between electrons and holes.[32,33] We evaluate the electronic band structure of GALs using a third nearest-neighbor tight-binding method. By introducing the antidots in the graphene sheet, the zero band-gap graphene can be converted into a narrowband-gap semiconductor[12,13] (see Fig. 2). This issue plays an important role in thermoelectric applications. In contrast to a pristine graphene sheet, GALs have a beneficial band-gap, so that one can suppress either the electron or the hole current to obtain unipolar conduction. For example, by adjusting the Fermi level near the conduction band the hole current will be negligible. The electron-hole asymmetry with respect to Fermi level depends on the band-gap, on the sharp features of transmission, on the width of the first conduction sub-band and on the value of the transmission. At room temperature, the width of the thermal broadening is about 0.2 eV. Therefore, a band-gap around 0.2 eV and a first conduction sub-band width larger than 0.2 eV will be ideal for thermoelectric applications. In Right-Tri(10,126), there are some localized midgap states, see Fig. 2(f), as a result of sublattice-symmetry breaking.[25,34] They have a zero group velocity and cannot contribute to the carrier transport. Although RightTri(10,126) has the sharpest features in the transmission and its transport band-gap is about 0.4 eV, the width of the first conduction sub-band of RightTri(10,126) is only 0.12 eV. As a result, it has a high Seebeck coefficient and a low electrical conductance, see Fig. 3. The first conduction sub-band of a Rect(10,120) has a non-zero group velocity. Therefore, we consider the rectangular GAL as a zero band-gap material and as a result, the Seebeck coefficient will be small, which is detrimental to thermoelectric applications. In a Hex(10,120), the first conduction and valence sub-bands are quasi-flat bands due to existence of some edge carbon atoms, which have only one nearest neighbor.[34] As shown in Fig. 2(d), these bands have a small group velocity and they have a small contribution to electron transport. As a result, the maximum value of Seebeck

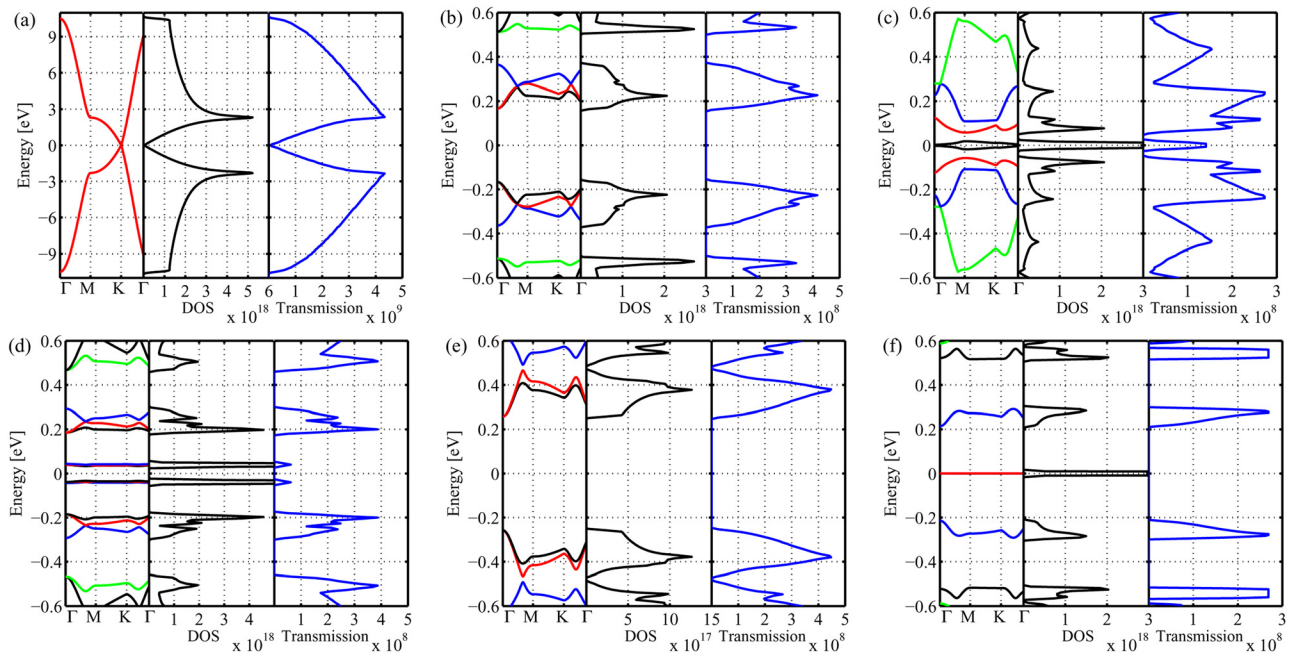

FIG. 2. (Color online) The electronic band structure along high symmetry lines. The density of states and transmission of (a) graphene sheet, (b) Circ(10,108), (c) Rect(10,120), (d) Hex(10,120), (e) IsoTri(10,126), and (f) RightTri(10,126). The units of the DOS and transmission are [eV^{-1} m^{-2}] and [m^{-1}], respectively.

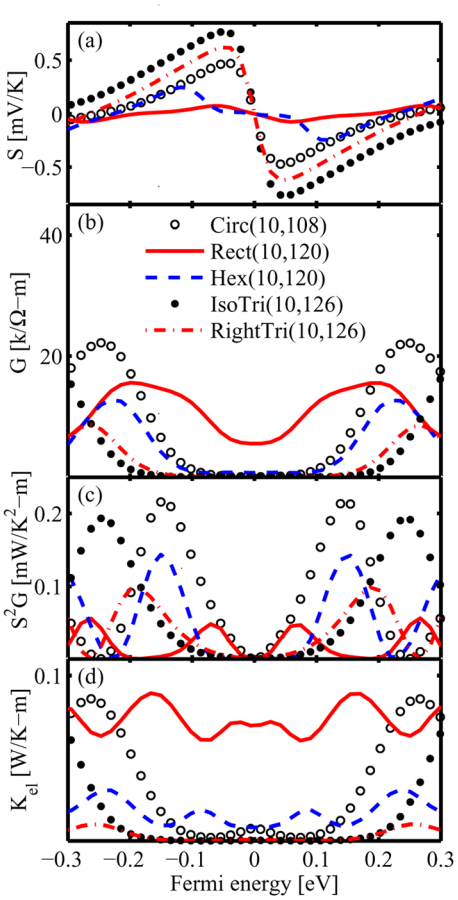

FIG. 3. (Color online) (a) Seebeck coefficient, (b) electrical conductance, (c) power factor, and (d) electrical thermal conductance as a function of the Fermi level.

coefficient of Hex(10,120) is not very large and it is located close to the band-edge of the second conduction sub-band. On the other hand, the electrical conductivity peaks close to the second sub-band-edge. Therefore, Hex(10,120) has the third highest power factor among the GALs with different antidot shapes.

On the other hand, the band-gap and the first conduction sub-band width of Circ(10,108) and IsoTri(10,126) are nearly 0.4 eV and 0.2 eV, respectively. They also have the highest transmissions. Therefore, as shown in Fig. 3, they are the best thermoelectric GALs in terms of the power factor. Because of a sharp feature in the transmission, Circ(10,108) has the highest power factor of the GALs considered. In addition, as shown in Fig. 3(d) the electron contribution to the thermal conductance can be neglected in comparison with the lattice thermal conductance (see Table III).

Next, we compare the thermal conductance of circular GALs with $L = 10$ and different radii, including Circ(10,24), Circ(10,108), and Circ(10,258). The phonon density of states (DOS) and phonon transmission of these GALs are shown in

TABLE III. The comparison of the thermal conductance of pristine graphene and different GALs.

Structure	Thermal conductance [W/K-m]
Pristine Graphene	1.3813
Circ(10, 24)	0.6948
Circ(10, 108)	0.3764
Circ(10, 258)	0.2220
Rect(10, 120)	0.3378
Hex(10, 120)	0.3764
IsoTri(10, 126)	0.2606
RightTri(10, 126)	0.2509

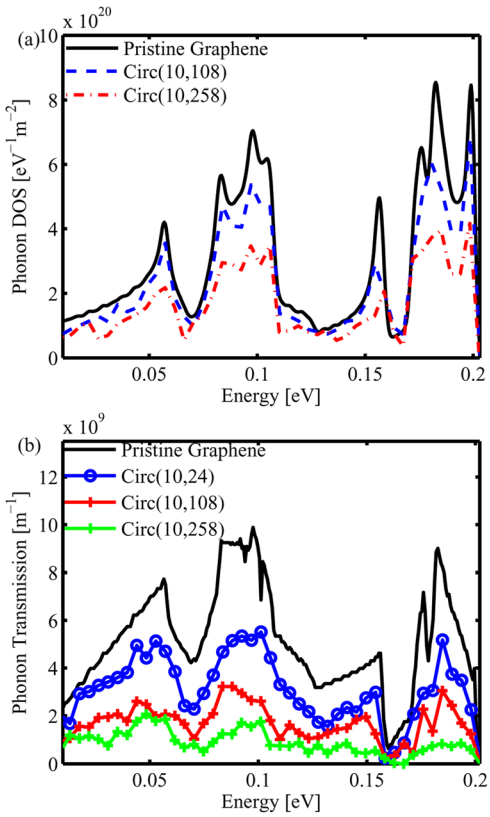

FIG. 4. (Color online) The comparison between (a) phonon density of states and (b) transmission of pristine graphene and circular GALs with different antidot areas.

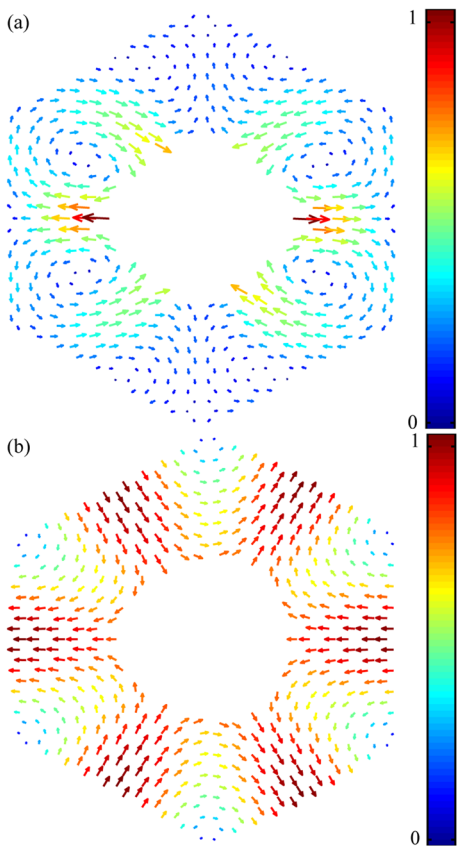

FIG. 5. (Color online) Phonon modes at Γ point: (a) represents a localized mode at $E = 30$ meV and (b) represents a propagating mode at $E = 16$ meV. The amplitude of vibrations has been normalized.

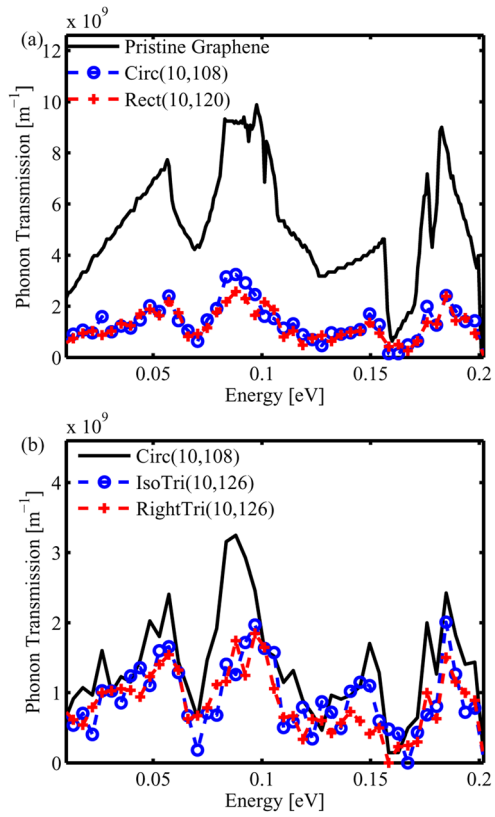

FIG. 6. (Color online) (a) The comparison between the phonon transmission of a pristine graphene, Circ(10,108), and Rect(10,120). (b) The comparison between the phonon transmission of Circ(10,108), IsoTri(10,126), and RightTri(10,126). IsoTri(10,126), and RightTri(10,126) have similar transmission, but generally smaller than that of Circ(10,108). This can be explained by a larger circumference and a lower distance between the nearest-neighbor antidots of these two GALs.

Fig. 4. As indicated in Table III, by increasing the size of the antidot, the phonon DOS, the phonon transmission, and the thermal conductance are significantly reduced. In Fig. 5 two phonon modes of Circ(10,108) at the Γ point are shown. Figure 5(a) presents a localized phonon mode as a result of introducing antidots, whereas, Fig. 5(b) shows a propagative mode. By introducing antidots into the graphene sheet, some phonon modes become localized, similar to electrons, and they cannot contribute to the thermal conductance.

To investigate the effect of the antidot circumference, we compare GALs with nearly the same area and different shapes, including Circ(10,108), Rect(10,120), Hex(10,120), IsoTri(10,126), and RightTri(10,126). Although the DOS of these GALs have the same order as that of a pristine graphene sheet, the transmissions can be very different. Figure 6(a) shows that the phonon transmissions of Circ(10,108) and Rect(10,120) are quite different from that of pristine graphene. However, Circ(10,108), Rect(10,120), and Hex(10,120) have nearly the same transmissions, whereas IsoTri(10,126) and Right(10,126) have similar transmissions that are different from the first group, see Fig. 6(b).

The transmissions of Circ(10,108), Rect(10,120), and Hex(10,120) are similar because they have similar circumference and thus the same number of boundary carbon atoms. Furthermore, the nearest-neighbor dots in these GALs have

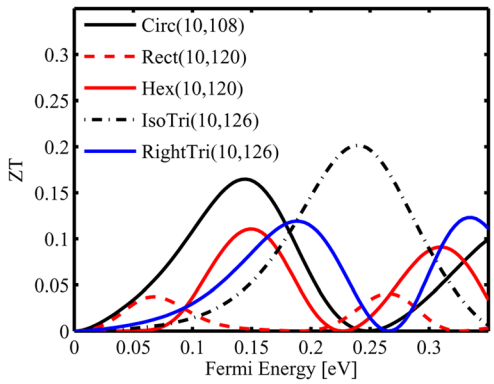

FIG. 7. (Color online) The figure of merit *ZT* of different GALs as a function of the Fermi energy.

nearly the same distance. On the other hand, IsoTri(10, 126) and RightTri(10, 126) have the same circumference that is different from those of the first group.

The thermal conductances of pristine graphene and different GALs are summarized in Table III. Triangular GALs have the smallest thermal conductance, although they have the minimum area of all antidot shapes. This behavior can be explained by considering the fact that triangular antidots have the highest circumference of all antidots with the same area. This indicates that circumference of the antidot has a stronger effect on the thermal conductance rather than its area.

The figures of merit of different GALs as a function of the Fermi energy are compared in Fig. 7. IsoTri has the highest *ZT*, because it has the lowest lattice thermal conductance and one of the largest Seebeck coefficient. At room temperature, the factor $\partial f/\partial E$ has significant values only in the range of 0.2 eV around the Fermi level. Under the condition $E_G > 0.2$ eV, holes have no contribution to the total electrical current. A large value of the Seebeck coefficient is therefore obtained.

In our work we did not consider the passivation of dangling bonds at the edges. However, it has been shown that hydrogen passivation of dangling bonds results in further reduction of the thermal conductance.[24] Therefore, a higher *ZT* for GALs can be obtained by edge passivation.

V. CONCLUSIONS

We numerically analyzed the ballistic thermoelectric properties of GALs. Our results indicate that the size of the antidots, the circumference of the antidots, and the distance between antidots can strongly influence the thermal properties of GALs. Resulting from ballistic calculation, we show that by appropriate selection of the geometrical parameters one can significantly reduce the thermal conductance of GALs and improve their thermoelectric figure of merit. This allows one to design and optimize the efficiency of graphene-based thermoelectric devices for future energy harvesting and other thermoelectric applications.

ACKNOWLEDGMENTS

This work, as part of the ESF EUROCORES program EuroGRAPHENE, was partly supported by funds from FWF, Contract No. I420-N16.

[1]G. Nolas, J. Sharp, and H. Goldsmid, *Thermoelectrics: Basic Principles and New Materials Developments* (Springer, New York, 2001), Chap. Historical Development.
[2]H. Goldsmid, *Introduction to Thermoelectricity* (Springer, New York, 2010), Chap. Review of Thermoelectric Materials.
[3]L. Weber and E. Gmelin, Appl. Phys. A **53**, 136 (1991).
[4]A. I. Hochbaum, R. Chen, R. D. Delgado, W. Liang, E. C. Garnett, M. Najarian, A. Majumdar, and P. Yang, Nature (London) **451**, 163 (2008).
[5]A. Boukai, Y. Bunimovich, J. Tahir-Kheli, J.-K. Yu, W. Goddard, and J. Heath, Nature (London) **451**, 168 (2008).
[6]R. Venkatasubramanian, E. Siivola, T. Colpitts, and B. O'Quinn, Nature **413**, 597 (2001).
[7]T. C. Harman, P. J. Taylor, M. P. Walsh, and B. E. LaForge, Science **297**, 2229 (2002).
[8]K. Novoselov, A. Geim, S. Morozov, D. Jiang, Y. Zhang, S. Dubonos, I. Grigorieva, and A. Firsov, Science **306**, 666 (2004).
[9]J.-H. Chen, C. Jang, S. Xiao, M. Ishighami, and M. Fuhrer, Nature Nanotech. **3**, 206 (2008).
[10]J. H. Seol, I. Jo, A. L. Moore, L. Lindsay, Z. H. Aitken, M. T. Pettes, X. Li, Z. Yao, R. Huang, D. Broido, N. Mingo, R. S. Ruoff, and L. Shi, Science **328**, 213 (2010).
[11]M. Han, B. Özyilmaz, Y. Zhang, and P. Kim, Phys. Rev. Lett. **98**, 206805 (2007).
[12]T. G. Pedersen, C. Flindt, J. Pedersen, A.-P. Jauho, N. A. Mortensen, and K. Pedersen, Phys. Rev. B **77**, 245431 (2008).
[13]A. Zhang, H. F. Teoh, Z. Dai, Y. P. Feng, and C. Zhang, Appl. Phys. Lett. **98**, 023105 (2011).
[14]A. Zhang, Y. Wu, S.-H. Ke, Y. Feng, and C. Zhang, arXiv:1105.5858 (2011).
[15]T. G. Pedersen, C. Flindt, J. Pedersen, N. A. Mortensen, A. P. Jauho, and K. Pedersen, Phys. Rev. Lett. **100**, 136804 (2008).
[16]J. Bai, X. Zhong, S. Jiang, Y. Huang, and X. Duan, Nature Nanotech. **5**, 190 (2010).
[17]K. Kim, Y. Zhao, H. Jang, S. Lee, J. Kim, K. Kim, J.-H. Ahn, P. Kim, J.-Y. Choi, and B. Hong, Nature (London) **457**, 706 (2009).
[18]A. A. Balandin, S. Ghosh, W. Bao, I. Calizo, D. Teweldebrhan, F. Miao, and C. N. Lau, Nano Lett. **8**, 902 (2008).
[19]J. Hone, M. Whitney, C. Piskoti, and A. Zettl, Phys. Rev. B **59**, R2514 (1999).
[20]H. Sevincli and G. Cuniberti, Phys. Rev. B **81**, 113401 (2010).
[21]Z. Guo, D. Zhang, and X.-G. Gong, Appl. Phys. Lett. **95**, 163103 (2009).
[22]Y. Ouyang and J. Guo, Appl. Phys. Lett. **94**, 263107 (2009).
[23]H. Zhang, G. Lee, A. F. Fonseca, T. L. Borders, and K. Cho, J. Nanomater. 2010, 537657 (2010).
[24]W. Evans, L. Hu, and P. Keblinski, Appl. Phys. Lett. **96**, 203112 (2010).
[25]J. Furst, J. Pedersen, C. Flindt, N. Mortensen, M. Brandbyge, T. Pedersen, and A.-P. Jauho, New J. Phys. **11**, 095020 (2009).
[26]S. Datta, *Quantum Transport: From Atoms to Transistors* (Cambridge University Press, Cambridge, 2005).
[27]D. Gunlycke and C. White, Phys. Rev. B **77**, 115116 (2008).
[28]R. Saito, T. Takeya, T. Kimura, G. Dresselhaus, and M. S. Dresselhaus, Phys. Rev. B **57**, 4145 (1998).
[29]R. Landauer, IBM J. Res. Dev. **1**, 223 (1957).
[30]C. Jeong, R. Kim, M. Luisier, S. Datta, and M. Lundstrom, J. Appl. Phys. **107**, 023707(2010).
[31]R. Kim, S. Datta, and M. S. Lundstrom, J. Appl. Phys. **105**, 034506 (2009).
[32]D. K. C. Macdonald, *Thermoelectricity: An Introduction to the Principles* (Dover, New York, 2006).
[33]J. Hone, I. Ellwood, M. Muno, A. Mizel, M. L. Cohen, and A. Zettl, Phys. Rev. Lett. **80**, 1042 (1998).
[34]M. Vanevic, V. M. Stojanovic, and M. Kindermann, Phys. Rev. B **80**, 045410 (2009).
[35]R. Saito, G. Dresselhaus, and M. Dresselhaus, *Physical Properties of Carbon Nanotubes* (Imperial College Press, London, 1998).